Supporting Information

The Design of Hierarchical Ternary Hybrid for Fiber-Shaped Asymmetric Supercapacitor with High Volumetric Energy Density

*Xunliang Cheng, Jing Zhang, Jing Ren, Ning Liu, Peining Chen, Ye Zhang, Jue Deng, Yonggang Wang, and Huisheng Peng**

State Key Laboratory of Molecular Engineering of Polymers, Collaborative Innovation Center of Polymers and Polymer Composite Materials, Department of Macromolecular Science, and Laboratory of Advanced Materials, Fudan University, Shanghai 200438, China; E-mail: penghs@fudan.edu.cn.

1. Experimental Section

1.1 Materials. Ordered microporous carbon (specific surface area of 900 $m^2 \cdot g^{-1}$, pore diameter of 3.8-4.0 nm) was purchased from the Nanjing XFNANO Materials Tech Co. Ltd., China. $Mn(NO_3)_2 \cdot 4H_2O$ and Poly(3,4-ethylenedioxythiophene):poly(styrene sulfonate) (PEDOT:PSS) were obtained from Sigma Aldrich. $NaNO_3$, Na_2SO_4, and carboxymethyl cellulose sodium were all provided by the Sinopharm Chemical Reagent, China.

1.2 Preparation of aligned CNT sheet. Aligned CNT sheets were dry-drawn from a CNT array that was synthesized by chemical vapor deposition at 740 ^oC with Fe (1.2 nm)/Al_2O_3 (3 nm) on a silicon substrate as the catalyst. The ethylene (flowing rate of 90 sccm) was used as the carbon source. A mixture of Ar (flowing rate of 400 sccm) and H_2 (flowing rate of 30 sccm) was used as the carrier gas.

1.3 Materials characterization. The surface morphologies and structures were characterized by the scanning electron microscope (SEM, Hitachi FE-SEM S-4800 operated at 1 kV). The energy-dispersive X-ray (EDX) elemental mappings were obtained on Bruker Xflash 6130 EDS system on a ZEISS EVO LS15 SEM set EHT at 20 KV. X-ray photoelectron spectroscopy (XPS) was recorded on an AXIS ULTRA DLD XPS System with MONO Al source (Shimadzu Corp.). Photoelectron spectrometer was recorded by using monochromatic Al KR radiation under vacuum at 5×10^{-9} Pa. All of the binding energies were referred to the C1s peak at 284.6 eV of the surface adventitious carbon.

1.4 Electrochemical Measurements. All electrochemical measurements, including the galvanostatic charge-discharge profiles, cyclic voltammograms, as well as cycling performance measurements were tested by a CHI 660a electrochemical workstation and an Arbin electrochemical station (MSTAT-5 V/10 mA/16Ch). The electrochemical performances of the electrode material were characterized with three-electrode system in 1 M Na_2SO_4 electrolyte solution. The as-fabricated electrode materials, saturated calomel electrode (SCE) and Pt wire serve as the working, reference and counter electrodes, respectively.

2. Calculation of Electrochemical Parameters

2.1 Single electrode. The specific volumetric capacitance (C_V) of a single electrode (positive or negative) was calculated from the galvanostatic charge-discharge curve based on the following equation:

$$C_v = \frac{I \times \Delta t}{V \times \Delta U}$$

where I, Δt, V, and ΔU are discharge current, discharge time, effective active material volume in the electrode and voltage window, respectively.

The C_V of the electrodes was also calculated from the CV curve by the following equation:

$$C_v = \frac{A}{2\,V \times S \times \Delta U}$$

where A, V, S, and ΔU are integral area of the CV curve, effective active material volume in the electrode, scan rate and voltage window, respectively.

The volume of the active material was calculated by assuming it as a cylinder. So the volume can be obtained by the following equation:

$$V = A \times L = \pi \times R^2 \times L$$

where A is the cross-sectional area of the fiber, R is the radius of the fiber, and L is the length of the fiber immersed into the electrolyte.

2.2 FAS. For the all-solid-state FAS, the specific volumetric capacitance of the whole device ($C_{cell,v}$) was calculated by the following equation:

$$C_{cell,v} = \frac{I \times \Delta t}{V_{cell} \times \Delta U}$$

where V_{cell} refers to the whole device volume, including the volume of two fibers and the surrounding electrolyte. The other symbols are the same as above.

According to the equation of $E = 0.5 \times C \times \Delta U^2$, the volumetric energy density (E_v) and volumetric power density (P_v) were calculated from the galvanostatic charge-discharge curves at different current densities using the following equations:

$$E_V = C_{cell,V} \times \Delta U^2/2 \times 3600$$

$$P_V = E_V \times 3600/\Delta t.$$

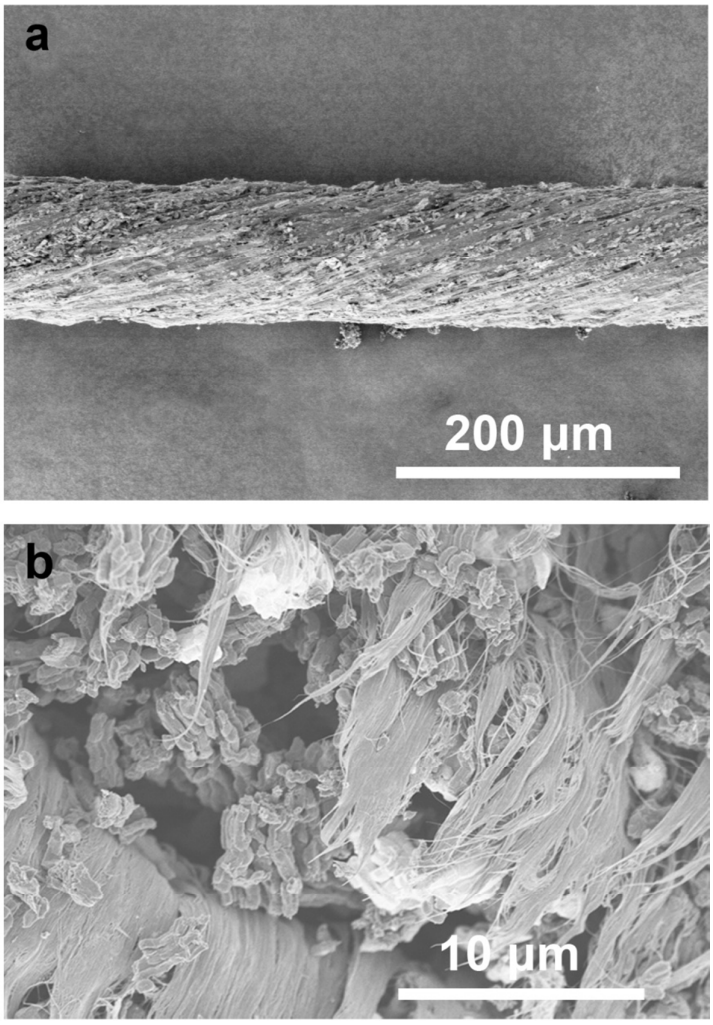

Figure S1. SEM images of the OMC/CNT hybrid fiber by (a) side and (b) cross-sectional views, respectively.

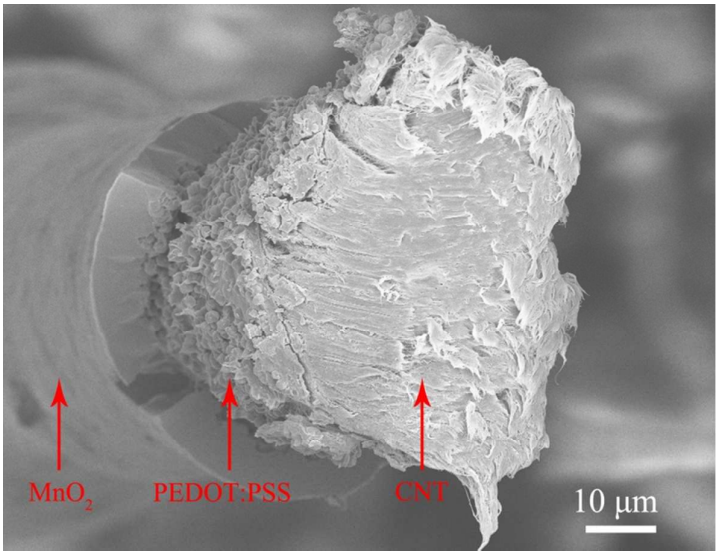

Figure S2. Cross-sectional SEM image of a MnO_2/PEDOT:PSS/CNT hybrid fiber.

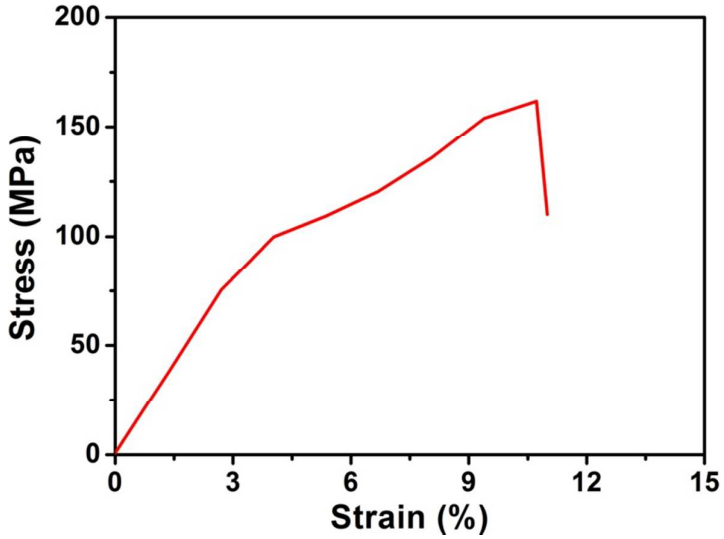

Figure S3. Stress-strain curve of the MnO_2/PEDO:PSS/CNT hybrid fiber.

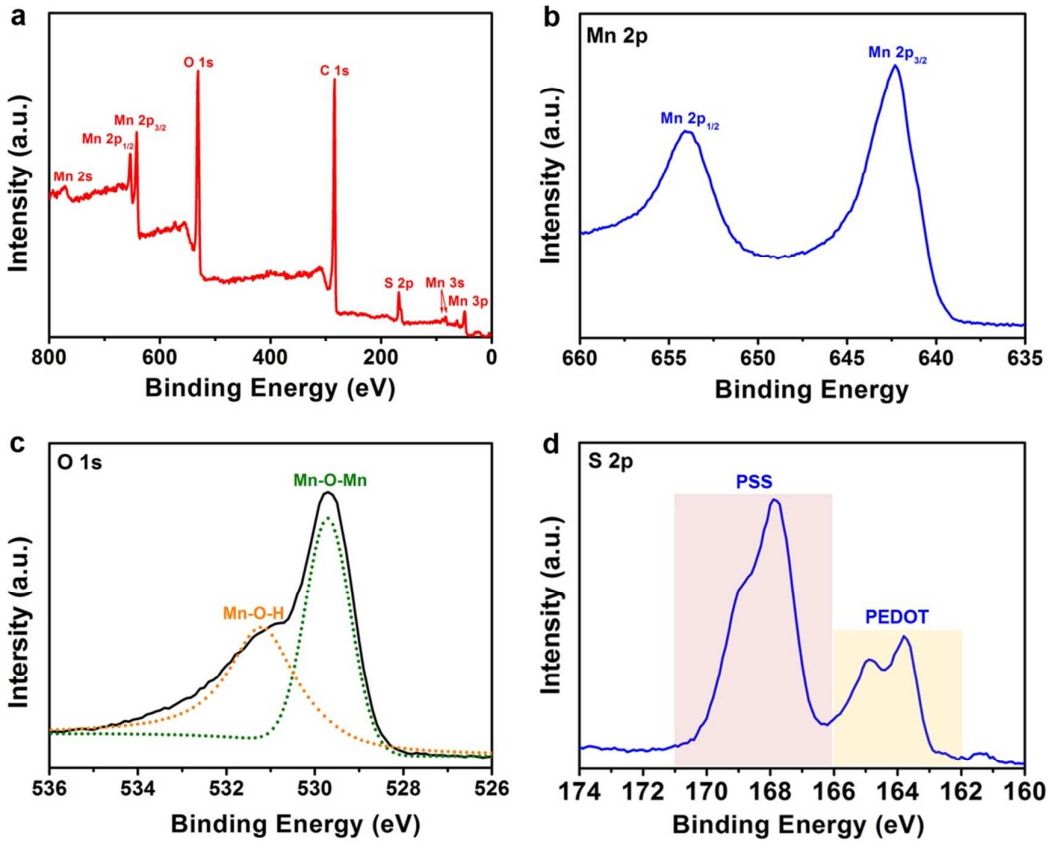

Figure S4. (a) XPS spectra of the MnO_2/PEDOT:PSS/CNT hybrid fiber. (b-d) XPS spectra of Mn 2p, O 1s, and S 2p, respectively.

The chemical composition of the ternary hybrid fiber was further characterized by XPS. As shown in Figure S2a, the C, O, Mn, and S elements can be clearly observed in the survey spectrum. The two peaks centered at the binding energy of 642.3 and 654.1 eV (Figure S2b) can be assigned to the binding energy of Mn $2p_{3/2}$ and Mn $2p_{1/2}$ with a spin-energy separation of 11.8 eV, while two peaks at 529.7 and 531.2 eV in the O 1s spectrum (Figure S2c) corresponds to Mn-O-Mn and Mn-O-H, respectively. These values are in accordance with the previous reports about MnO_2.[S1, S2] The S 2p XPS spectrum in Figure S2d also indicates the presence of PEDOT:PSS component in the hybrid fiber. The two XPS bands from 166 to 171 eV are the S 2p band of the sulfur atoms from the sulphonate group in PSS, whereas the two XPS bands between 162 and 166 eV are the S 2p band of the sulfur atoms from thiophene group in PEDOT.[S3, S4] The XPS spectra clearly demonstrate that the ternary hybrid fiber is composed of C, PEDOT:PSS, and MnO_2.

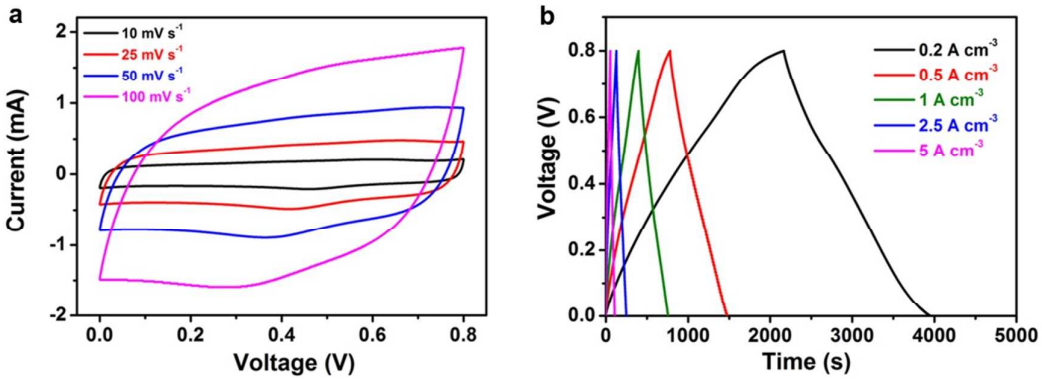

Figure S5. (a) CV curves of the MnO_2/PEDOT:PSS/CNT hibrid fiber collected at increasing scan rates. (b) Charge-discharge curves with increasing current densities.

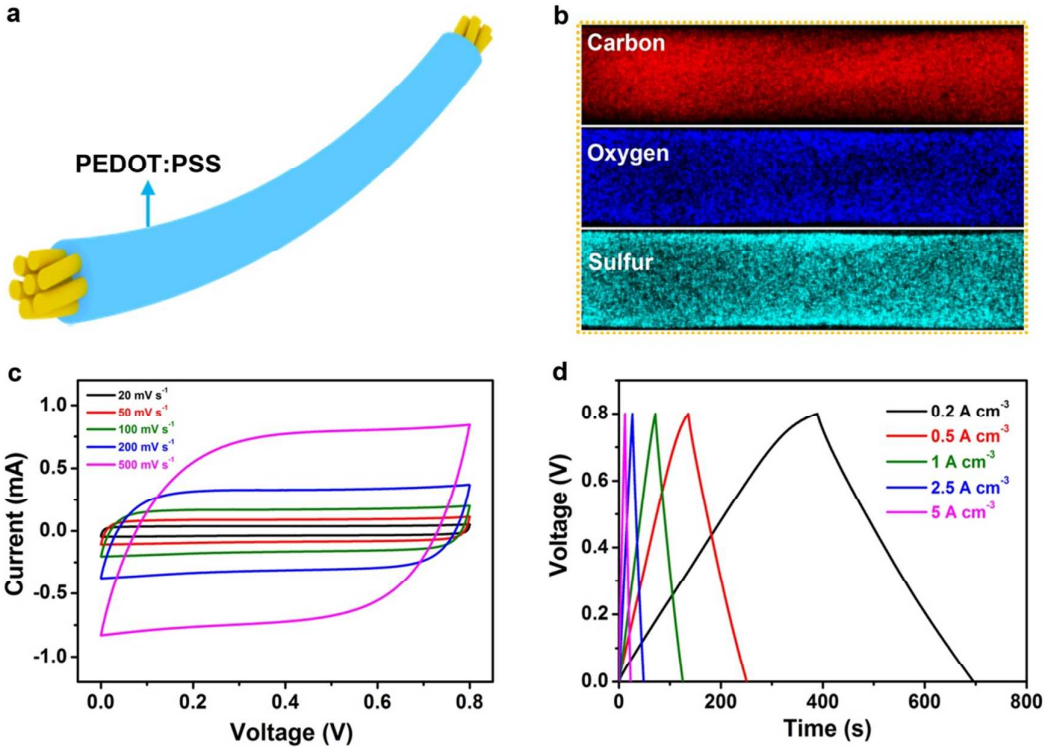

Figure S6. Characterization of PEDOT:PSS/CNT hybrid fiber. (a) and (b) Schematic illustration and EDS mapping, respectively. (c) CV curves at increasing scan rates. (d) Charge-discharge curves at increasing current densities.

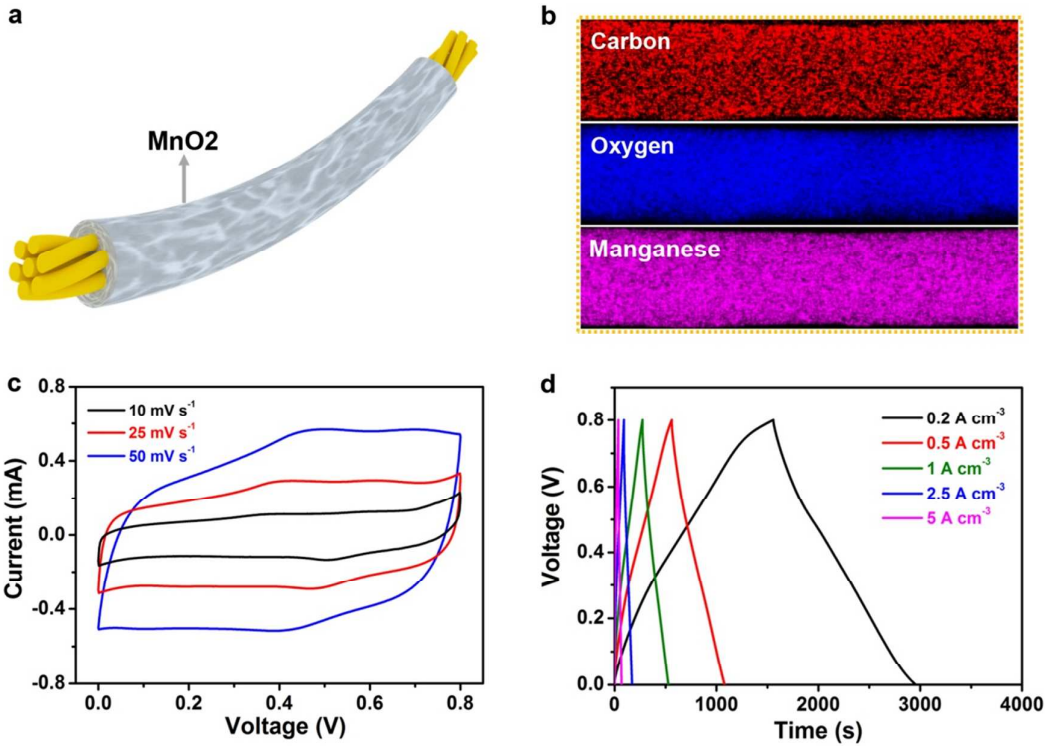

Figure S7. Characterization of MnO_2/CNT hybrid fiber. (a) and (b) Schematic illustration and EDS mapping, respectively. (c) CV curves at increasing scan rates. (d) Charge-discharge curves at increasing current densities.

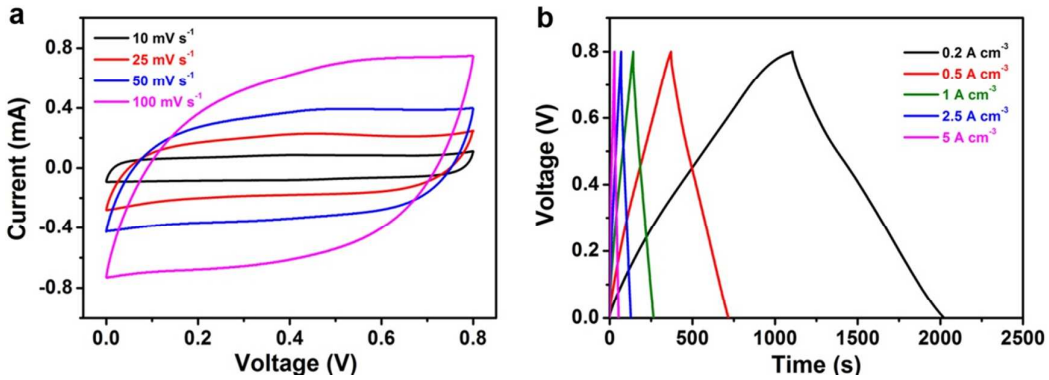

Figure S8. Characterization of PEDOT:PSS/MnO_2/CNT hybrid fiber. (a) CV curves at increasing scan rates. (b) Charge-discharge curves at increasing current densities.

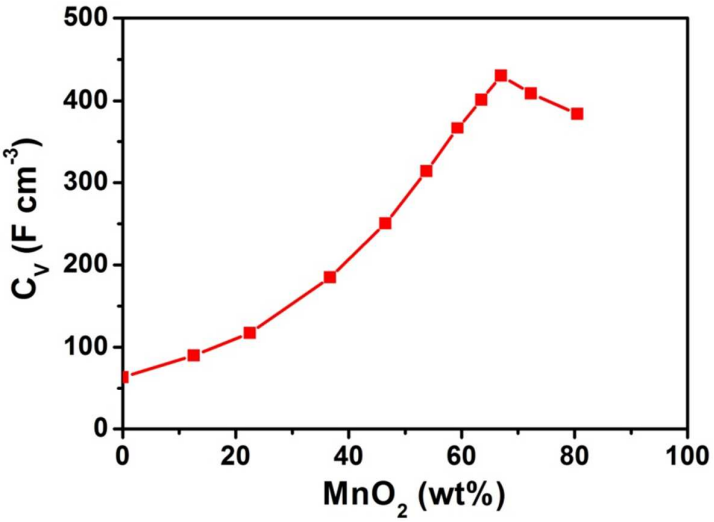

Figure S9. Dependence of specific volumetric capacitance on weight percentage of MnO_2 in the ternary hybrid fiber measured at 0.2 A·cm^{-3}.

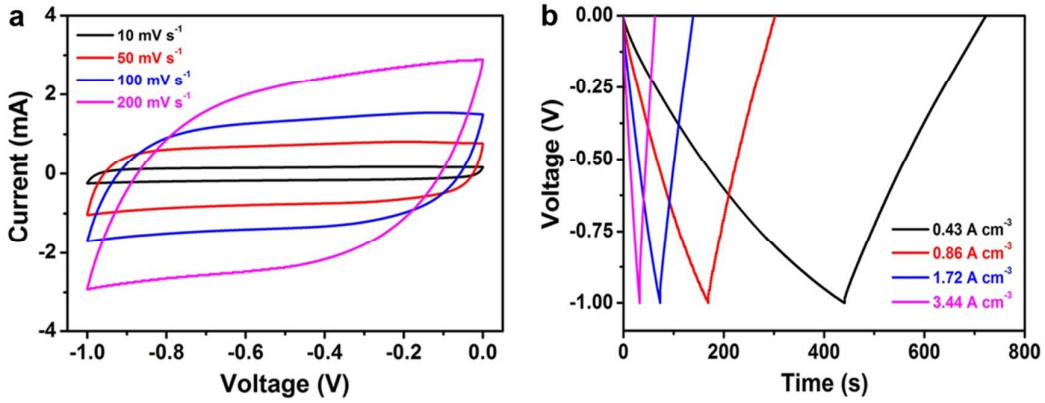

Figure S10. (a) CV curves of OMC/CNT nagative electrode at scan rates between -1.0 and 0 V. (b) Charge-discharge curves with increasing current densities.

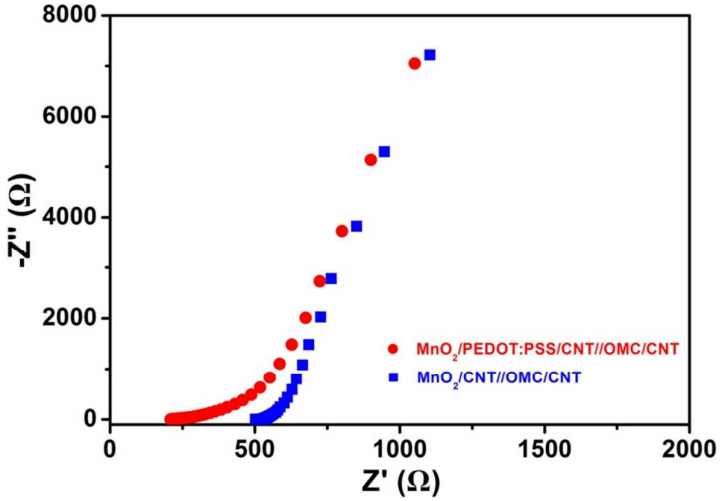

Figure S11. Electrochemical impedance spectra of the two different FAS devices in the frequency ranging from 0.1 to 100 kHz.

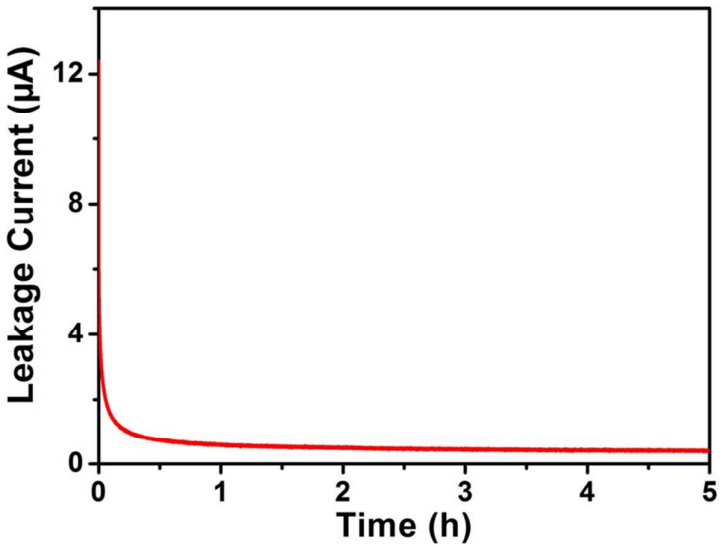

Figure S12. Leakage current measurement of the FAS.

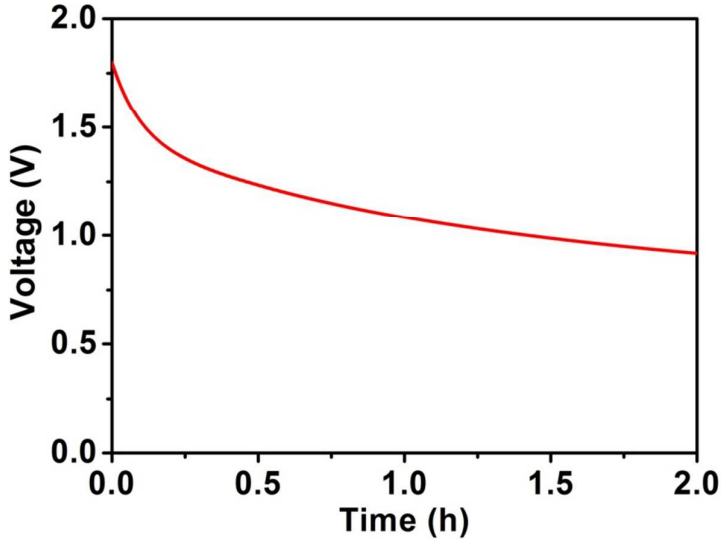

Figure S13. Self-discharge test of the FAS. It was charged at 1×10^{-4} A and then rested for 2 h.

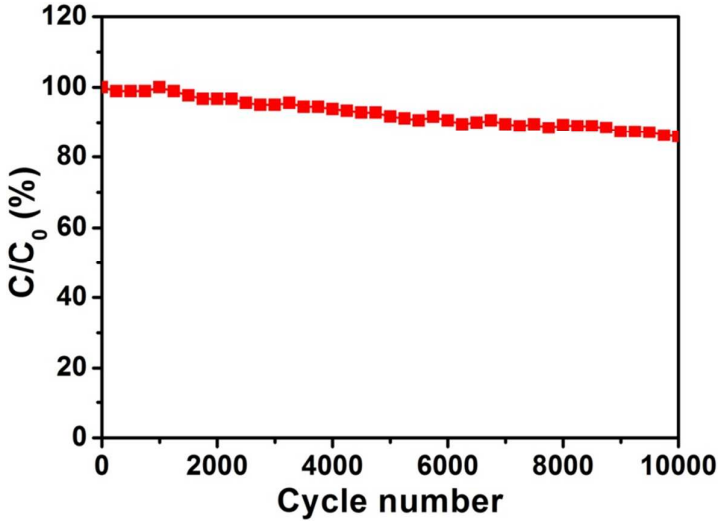

Figure S14. Cycling behavior of the FAS at a current density of 1.36 A·cm^{-3}.

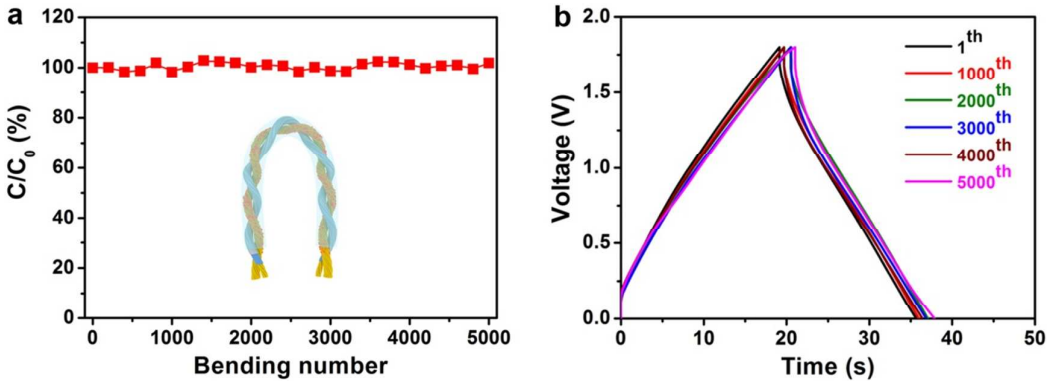

Figure S15. (a) Dependence of specific volumetric capacitance on bending cycle number. Here C and C_0 correspond to the specific capacitances before and after bending for different times, respectively. (b) Charge and discharge curves after different bending cycles.

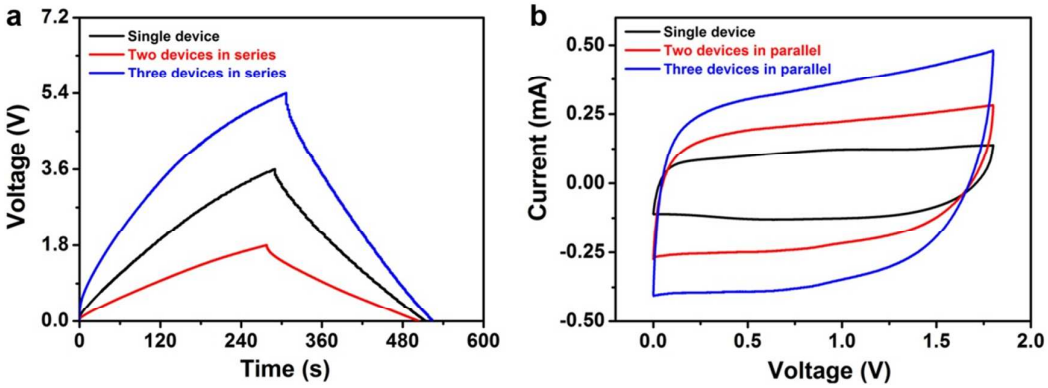

Figure S16. (a) Charge-discharge curves of three FASs connected in series. (b) CV curves of one FAS and two and three FASs connected in parallel. The scan rate was 20 $mV \cdot s^{-1}$.

References for the Supporting Information

S1 Zhang, Z.; Xiao, F.; Xiao, J.; Wang, S. Functionalized carbonaceous fibers for high performance flexible all-solid-state asymmetric supercapacitors. *J. Mater. Chem. A* **2015**, *3*, 11817-11823.

S2 Yu, N.; Yin, H.; Zhang, W.; Liu, Y.; Tang, Z.; Zhu, M. Q. High-Performance Fiber-Shaped All-Solid-State Asymmetric Supercapacitors Based on Ultrathin MnO_2 Nanosheet/Carbon Fiber Cathodes for Wearable Electronics. *Adv. Energy Mater.* **2016**, *6*, 1501458.

S3 Zhou, J.; Li, E. Q.; Li, R.; Xu, X.; Ventura, I. A.; Moussawi, A.; Anjum, D. H.; Hedhili, M. N.; Smilgies, D.-M.; Lubineau, G. Semi-Metallic, Strong And Stretchable Wet-Spun Conjugated Polymer Microfibers. *J. Mater. Chem. C* **2015**, *3*, 2528-2538.

S4 Kim, G.; Shao, L.; Zhang, K.; Pipe, K. P. Engineered Doping of Organic Semiconductors for Enhanced Thermoelectric Efficiency. *Nat. Mater.* **2013**, *12*, 719-723.